AGU PUBLICATIONS

JGR

Journal of Geophysical Research: Earth Surface

RESEARCH ARTICLE

10.1002/2013JF002751

Key Points:
- Self-organized shoreline sand waves develop with a characteristic wavelength
- Wave transformation over the undulating bathymetry causes wavelength selection
- The wavelength scales with offshore water wavelength divided by shoreface slope

Correspondence to:
F. Ribas,
francesca.ribas@upc.edu

Citation:
van den Berg, N., A. Falqués, F. Ribas, and M. Caballeria (2014), On the mechanism of wavelength selection of self-organized shoreline sand waves, *J. Geophys. Res. Earth Surf.*, *119*, 665–681, doi:10.1002/2013JF002751.

Received 5 FEB 2013
Accepted 18 FEB 2014
Accepted article online 20 FEB 2014
Published online 26 MAR 2014

On the mechanism of wavelength selection of self-organized shoreline sand waves

N. van den Berg[1], A. Falqués[1], F. Ribas[1], and M. Caballeria[2]

[1]Applied Physics Department, Universitat Politècnica de Catalunya, BarcelonaTech, Barcelona, Spain, [2]Escola Politècnica Superior, Universitat de Vic, Vic, Spain

Abstract Sandy shorelines exposed to very oblique wave incidence can be unstable and develop self-organized shoreline sand waves. Different types of models predict the formation of these sand waves with an initially dominant alongshore wavelength in the range 1–10 km, which is quite common in nature. Here we investigate the physical reasons for such wavelength selection with the use of a linear stability model. The existence of a minimum wavelength for sand wave growth is explained by an interplay of three physical effects: (a) largest relative (to the local shoreline) wave angle at the downdrift flank of the sand wave, (b) wave energy concentration at the updrift flank due to less refractive energy dispersion, and (c) wave energy concentration slightly downdrift of the crest due to refractive focusing. For small wavelengths, effects (a) and (c) dominate and cause decay, while for larger wavelengths, effect (b) becomes dominant and causes growth. However, the alongshore gradients in sediment transport decrease for increasing wavelength, making the growth rate diminish. There is therefore a growth rate maximum giving a dominant wavelength, L_M. In contrast with previous studies, we show that L_M scales with λ_0/β (λ_0 is the wavelength of the offshore waves and β is the mean shoreface slope, from shore to the wave base), an estimate of the order of magnitude of the distance waves travel to undergo appreciable transformation. Our model investigations show that the proportionality constant between L_M and λ_0/β is typically in the range 0.1–0.4, depending mainly on the wave incidence angle.

1. Introduction

Shoreline sand waves are undulations of the shoreline that extend into the bathymetry up to depths of O (10 m). Here we focus on sand waves that occur at length scales of O (1–10 km) and time scales of O (1–10 yr), and which are not directly related to surf zone rhythmic bars (the latter occurring at length scales of O (0.1–1 km) and time scales of O (1–10 days)). These shoreline sand waves are episodically or persistently found along many sandy coasts [*Bruun*, 1954; *Verhagen*, 1989; *Inman et al.*, 1992; *Thevenot and Kraus*, 1995; *Gravens*, 1999; *Guillen et al.*, 1999; *Stive et al.*, 2002; *Ruessink and Jeuken*, 2002; *Davidson-Arnott and van Heyningen*, 2003; *Medellín et al.*, 2008; *Alves*, 2009; *Caballeria et al.*, 2011; *Ryabchuk et al.*, 2011; *Kaergaard et al.*, 2012; *Ribas et al.*, 2013]. They could be triggered by different physical mechanisms, including forcing by offshore bathymetric anomalies or input of large quantities of sand from inlets and rivers [*Thevenot and Kraus*, 1995], but they can also emerge from irregularities of an otherwise rectilinear coast in absence of any evident forcing at their specific wavelength. The latter can occur if the wave climate is dominated by high-angle waves (i.e., waves with a high incidence angle relative to the shore normal), which make a rectilinear coast unstable [*Ashton et al.*, 2001; *Falqués and Calvete*, 2005; *Ashton and Murray*, 2006a; *van den Berg et al.*, 2011, 2012; *Kaergaard and Fredsoe*, 2013]. We will refer to this phenomenon as high-angle wave instability (HAWI from now on) and to the corresponding shoreline pattern as free or self-organized sand waves. Examples of observed shoreline sand waves of small amplitude are shown in Table 1. The critical water wave angle for instability is about 45° at the depth of closure, i.e., at the most offshore reach of the shoreline-associated bathymetric perturbations [*van den Berg et al.*, 2012].

Cuspate forelands and spits at larger length scales O (10–10^2 km) have also been reported in connection with high-angle wave climates, in addition to shoreline sand waves [*Ashton and Murray*, 2006b; *Ashton et al.*, 2009; *Alves*, 2009; *Ribas et al.*, 2013]. These large-scale features may coexist with sand waves (e.g., along the coast of Namibia) [see *Ribas et al.*, 2013] and may have evolved from shoreline sand waves by the nonlinear processes described in *Ashton et al.* [2001] and *Ashton and Murray* [2006a], which are beyond the scope of

Table 1. Wavelength of Self-Organized Shoreline Sand Waves[a] Along Several Coasts

Location	Reference	Wavelength (km)
Fire Island, U.S. East Coast	*Gravens* [1999]	1–2
Dutch coast	*Ruessink and Jeuken* [2002]	3.5–10
Santander Bay, Spain	*Medellín et al.* [2008]	0.12–0.15
Catalan coast, Spain	*Caballeria et al.* [2011]	1–1.5
Denmark East Coast	*Kaergaard et al.* [2012]	5–6
SW African coast	*Ribas et al.* [2013]	2–8

[a]Only small-amplitude shoreline sand waves at the length scales of kilometers are included.

the present paper (i.e., finite amplitude behavior). Here we focus on the initial stages of self-organized sand wave formation.

The first modeling study on HAWI did not predict any most preferred wavelength [*Ashton et al.*, 2001]. Furthermore, there was no lower limit on the growing wavelengths. *Falqués and Calvete* [2005] showed that the absence of wavelength selection occurred because the model of *Ashton et al.* [2001] did not take the curvature of bathymetric contours into account. If this is accounted for into the wave transformation from deep water up to breaking, there is a lower limit on the wavelength, L_c (called cutoff wavelength), below which sand waves do not grow; therefore, an initially dominant wavelength L_M emerges. This wavelength selection was first obtained with linear stability models [*Falqués and Calvete*, 2005; *Uguccioni et al.*, 2006] but it has also been confirmed recently with nonlinear morphodynamic models [*van den Berg et al.*, 2012; *Kaergaard and Fredsoe*, 2013]. The value of L_M depends on a number of factors such as the cross-shore profile of the shoreface and the wave height, period and angle. *Falqués and Calvete* [2005] obtained a range $L_M \sim 3$–15 km by examining mild surf zone bottom slopes in the range 0.005–0.02, whereas *van den Berg et al.* [2012] obtained wavelengths about 2–5 km for a surf zone slope of 0.03. For steeper beaches, wavelengths in the range 0.6–1.5 km may appear [*Caballeria et al.*, 2011], and even shorter wavelengths of 100–200 m can exceptionally occur in case of a very steep beach and very particular wave conditions [*Medellín et al.*, 2009]. Thus, the wavelength selection for self-organized shoreline sand waves is a robust output of the models provided that the curvature of the bathymetric contours is not ignored. Furthermore, this wavelength selection in the range 1–10 km is coherent with field observations of self-organized sand waves, as can be seen in Table 1.

The physical reasons for the existence of a dominant wavelength at the initial development of HAWI have only been recently explored. As a preliminary step, *Falqués and Calvete* [2005] made some computations for very short sand waves and showed that in that case there was a strong increase of wave refraction at the lee of the sand wave, bringing the maximum in wave energy from updrift to downdrift of the crest. As a result the short sand waves decay, and there is a lower limit for the emerging wavelengths (minimum wavelength) [*Falqués et al.*, 2011]. *van den Berg et al.* [2012] recently showed that there is a shift from the dominance of wave energy focusing at the crest for small wavelengths to the dominance of wave energy spreading for large wavelengths. This leads to an alongshore transport pattern that shifts from diffusion to growth of the shoreline undulations when increasing their wavelength. At the same time, the gradients in alongshore transport decrease for increasing wavelength, leading to decreasing growth rates. This explains the existence of a wavelength of maximum growth (dominant wavelength) [*van den Berg et al.*, 2012].

The first aim of the present contribution is to further quantify the physical mechanism that explains the existence of a dominant wavelength for the initial development of HAWI, and thereby, a wavelength selection for self-organized shoreline sand waves. The second aim is to find out how the wavelength depends on the bathymetric and wave conditions. The computations of *Falqués and Calvete* [2005] and *Uguccioni et al.* [2006] suggested that the wavelength scales with the width of the surf zone, X_b, with a large factor ranging from 50 to 200. However, this is intriguing since the water wave transformations that control the sediment transport rate in the models occur before breaking. Furthermore, the large ratio between the wavelength and X_b suggests that X_b does not control the physical processes that are responsible for the wavelength selection. A more probable dependence seems to exist between the wavelength and the shoreface slope (suggested by both computations and observations). Thus, there is a need for a systematic exploration of

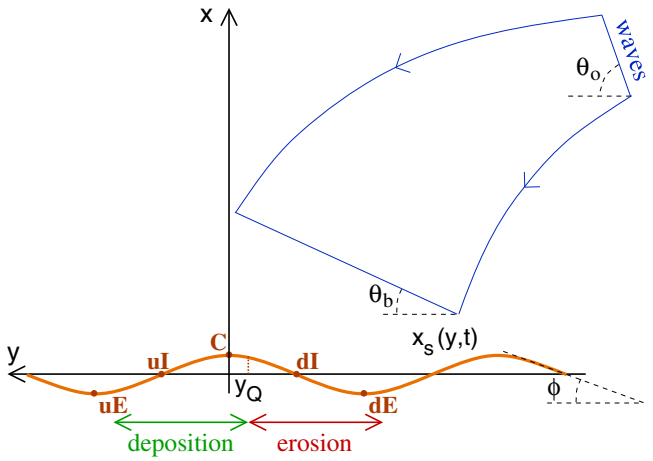

Figure 1. Sketch of a sinusoidal sand wave, where the wave crest (C), the adjacent updrift and downdrift inflection points (uI and dI) and embayments (uE and dE), and the location of the maximum in sediment transport rate ($y=y_Q$) are shown. The situation where the gradients in Q cause growth and downdrift translation of the sand wave is represented. The coordinate system used and the different angles of the model equations are also shown.

the parametric trends of the dominant wavelength and also of its sensitivity to other parameters like wave height, period, and angle.

The linear stability model developed by *Falqués and Calvete* [2005] is used in the present study. In section 2, the governing equations and the methodology are presented. The behavior of the gradients in alongshore sediment transport as a function of the wavelength is investigated in section 3 in order to quantify the physical processes that are responsible for the wavelength selection. In section 4 an exploration is done to unravel the main parametric trends of the dominant wavelength. A discussion and the conclusions are presented in section 5.

2. Extended One-Line Shoreline Model

2.1. Governing Equations

The model used in this study is called 1-D morfo, and it was first presented in *Falqués and Calvete* [2005]. The model equations were described in detail in that paper and here we only explain their most important characteristics. A Cartesian reference frame is used, where y runs along the mean shoreline orientation, x runs seaward in the cross-shore direction, and z is directed upward (Figure 1). Since we are interested in coastal morphodynamics at large length and time scales under oblique wave incidence, we use the so-called one-line modeling approach where the changes in coastline position are simply caused by the gradients in the alongshore transport rate Q according to

$$\bar{D}\frac{\partial x_s}{\partial t} = -\frac{\partial Q}{\partial y}\,. \tag{1}$$

The shoreface bathymetry is given by $z = z_b(x, y, t)$ and the position of the shoreline is $x = x_s(y, t)$ where t is time. The porosity factor is included in Q for simplicity and $\bar{D}$ is the average active water depth. The latter quantity is of the order of the depth of closure, and it is computed by assuming sediment conservation in the cross-shore profile [*Falqués and Calvete*, 2005], i.e., any sediment deficit or excess on a cross-shore section induces a displacement of the shoreline.

The computation of the total transport rate Q (m^3/s) is commonly done with an empirical approach based on H_b and α_b, i.e., the (root-mean-square) wave height and the angle of the wave fronts with respect to the local shoreline orientation at breaking. Here we apply the widely used CERC formula [*Komar*, 1998],

$$Q = \mu H_b^{5/2}\sin(2\alpha_b)\,, \tag{2}$$

where μ is an empirical constant typically in the range 0.15–0.2 $m^{1/2}\,s^{-1}$ [*Falqués and Calvete*, 2005]. This constant is proportional to the parameter K_1 of the original CERC formula and the value we use, $\mu = 0.15$,

corresponds to $K_1 = 0.55$ (in case of using the values $\rho = 10^3$ kg/m^3 and $\rho_s = 2.65\ 10^3$ kg/m^3 for the water and sediment densities, $p = 0.4$ for the sediment porosity, and $\gamma_b = 0.5$ for the breaking index). Also, $\alpha_b = \theta_b - \phi$, where θ_b is the angle of the wave fronts at breaking and $\phi = \tan^{-1}(\partial x_s/\partial y)$ is the angle of the shoreline, both measured clockwise from the y axis (Figure 1). Other empirical expressions for Q are expected to give qualitatively similar results [*Ashton and Murray*, 2006b].

For a rectilinear coastline with parallel depth contours and in absence of alongshore gradients in deep water wave conditions, H_b and α_b are alongshore uniform so that there are no gradients in Q and the shoreline position is constant in time. If we introduce an undulation to the coastline, gradients arise in ϕ, which causes gradients in Q. According to equation (1) the new shoreline is no longer static. The changes in the shoreline position are linked to changes in the shoreface bathymetry that in turn cause changes in H_b and θ_b due to wave refraction. This feedback effect is the essential process behind HAWI [*Ashton et al.*, 2001] and it is ignored by the traditional one-line shoreline approach, which always predicts a diffusive behavior and therefore a stable shoreline [*Pelnard-Considère*, 1956]. Thus, H_b and θ_b cannot be considered constant along the coast but they must be computed from the offshore wave characteristics as a function of the changing bathymetry.

Given that the bathymetry is not a dynamic unknown of equation (1), the link between the shoreline and the bathymetry is done in a parametric way

$$z_b(x,y,t) = -D(x,y,t) = -D_0(x) + D_0(x_s(y,t))\, f(x - x_s(y,t))\,. \tag{3}$$

The unperturbed water depth is $D_0(x)$ with $D_0(0) = 0$ so that the unperturbed shoreline is located at $x = 0$. The function $f(x)$ gives the cross-shore shape of the bathymetric perturbation, and it satisfies $f(x=0) = 1$ and $f(x > x_c) = 0$, where x_c is the location of the depth of closure, D_c. The complete expression of $f(x)$ is specified in section 2.3. Notice that we assume that the bathymetry reacts instantaneously to shoreline changes and also that the offshore extent of the perturbation is finite and fixed in time.

Since we are interested in the basic parametric trends regarding the optimum wavelength of sand waves, we consider a simple description of water wave transformation including only the basic processes of refraction and shoaling. We consider the optical approximation for monochromatic water waves with wavelength λ_0, height H_0 and angle θ_0 in deep water, where the wave period T is used to compute $\lambda_0 = gT^2/(2\pi)$. Effects in wave forcing such as spreading of the wave direction and changes of wave properties with time are not accounted for. The transformation up to breaking is described with the dispersion relation,

$$\omega^2 = gk \tanh(kD)\,, \tag{4}$$

the wave number irrotationality,

$$\frac{\partial}{\partial x}(k \sin\theta) = \frac{\partial}{\partial y}(-k \cos\theta)\,, \tag{5}$$

and the energy conservation equation (up to breaking),

$$\frac{\partial}{\partial x}(-c_g H^2 \cos\theta) + \frac{\partial}{\partial y}(c_g H^2 \sin\theta) = 0\,. \tag{6}$$

Here, $\omega = \sqrt{2\pi g/\lambda_0}$ is the radian frequency, k is the wave number module, g is the gravity acceleration, θ is the angle of the wave crests measured clockwise from the y axis, and c_g is the group celerity.

The shoreline equation (1) and the sediment transport formula (2), which are linked to the bathymetry through equation (3), together with the wave transformation equations (4)–(6), constitute a complete set of equations that can be used to determine the unknowns $x_s(y,t)$, $D(x,y,t)$, $k(x,y,t)$, $\theta(x,y,t)$, and $H(x,y,t)$. In the context of the present study, the integration domain for the wave transformation equations is the region where $x \geq x_b(y,t)$, with x_b being the breaking line. The latter is defined by $H(x_b,y,t) = \gamma_b D(x_b,y,t)$, where a default value $\gamma_b = 0.6$ is used. Thereby, only the offshore wave conditions are needed,

$$k(\infty,y,t) = 2\pi/\lambda_0\,, \quad \theta(\infty,y,t) = \theta_0\,, \quad H(\infty,y,t) = H_0\,. \tag{7}$$

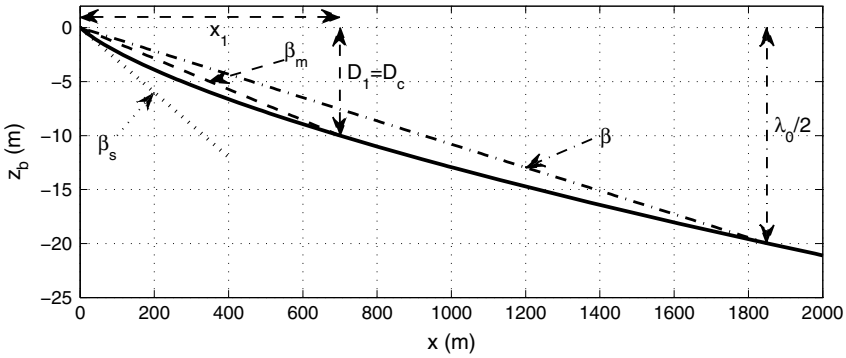

Figure 2. Default Dean-type profile with some of its parameters, defined in section 2.3.2. The two different slopes used in this study are also included: the shoreline slope, β_s, and the mean shoreface slope (averaged from shore to the wave base), β.

2.2. Methodology

Linear stability analysis is a powerful tool to explore the initial tendency of the morphodynamic system to develop sand waves due to HAWI. Since the details of this methodology were given in *Falqués and Calvete* [2005], we only outline the main aspects. Once the equilibrium reference state corresponding to a rectilinear shoreline has been computed, we assume a sinusoidal shoreline undulation,

$$x_s(y,t) = a\, e^{\sigma t + iKy} + c.c.\,, \tag{8}$$

where $A = 2a$ is the cross-shore amplitude and $L = 2\pi/K$ is the wavelength of the shoreline sand wave. The corresponding bathymetry follows from the linearization of equation (3) for $a \to 0$,

$$D(x,y,t) = D_0(x) - \beta_s\, f(x)\, x_s(y,t)\,, \tag{9}$$

where β_s is the slope of the bottom profile at the shoreline. The shape function $f(x)$ is specified in section 2.3. Once the perturbed bathymetry is defined, the wave transformation equations (4)–(6) are linearized for $a \to 0$ and the perturbed wave height and angle at breaking are obtained (this is not straightforward) [see *Falqués and Calvete*, 2005]. This allows for the computation of the linearized sediment transport rate (equation (2)). Finally, inserting equation (8) into equation (1) and linearizing leads to the computation of the complex growth rate, $\sigma = \sigma_r + i\sigma_i$ for each wavelength L. Perturbations with $\sigma_r > 0$ will grow in time and the wavelength L_M for which σ_r is maximum corresponds to the fastest growing sand wave, which is expected to be the dominant wavelength in nature in the initial stages of sand wave formation. The imaginary part gives the alongshore propagation celerity of the sand waves, according to $V = -\sigma_i/K$. It must be kept in mind that this analysis only gives the initial tendency of the system to develop free sand waves of a certain wavelength L. Consistency between the linear stability analysis and nonlinear modeling is therefore desirable. The main results of the present analysis compare well with the nonlinear modeling by *van den Berg et al.* [2012].

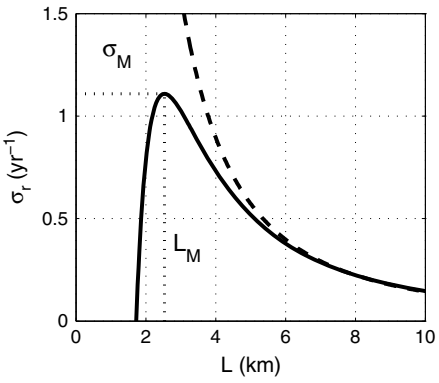

Figure 3. Typical modeled instability curve, with the real growth rate σ_r as a function of the wavelength L (solid line), for the Dean-type bathymetry and the parameter values of section 3 (Table 2). The dashed line represents the diffusional behavior, where $\sigma_r \propto L^{-2}$.

2.3. Model Setup

It is necessary to prescribe a bathymetric profile for the unperturbed situation and the cross-shore shape of the bathymetric perturbation. We apply two different shoreface bathymetries, which are specified in the following subsections.

2.3.1. Idealized Shoreface Bathymetry: Planar Profile

A planar shoreface, with constant slope β, provides the most simple bathymetric profile in the model,

$$D_0(x) = \beta x\,. \tag{10}$$

Table 2. Default Model Setup in the Runs of the Different Sections

Section	Profile	D_c	H_0(m)	θ_0(°)	T(s)	γ_b
3	Dean type	10	1.0	60	6	0.6
4.1	Planar	100	1.0	60	6	0.6
4.2	Dean type	10	1.0	60	6	0.6

Regarding the bathymetric perturbation, the most simple option is to assume that when the shoreline shifts offshore or onshore, the whole profile shifts accordingly, preserving its shape up to the depth of closure, D_c. This means that the shape function in equation (9) is of the form

$$f(x) = \begin{cases} 1 & \text{if} \quad x < x_c \\ 0 & \text{if} \quad x \geq x_c \end{cases} , \tag{11}$$

where $D_0(x_c) = D_c$. Notice that the perturbed profile has a small jump at $x = x_c$ but, as long as D_c is large enough in comparison with λ_0, its effect on wave transformation is not significant. The default values we use for this bathymetry are $\beta_m = 0.03$ and $D_c = 100$ m.

2.3.2. Realistic Shoreface Bathymetry: Dean-Type Profile

A more realistic shoreface profile is a Dean-type profile [*Komar*, 1998] of the form

$$D_0(x) = B\left((x+d)^{2/3} - d^{2/3}\right) , \tag{12}$$

where d introduces a small shift to avoid an infinite slope at the shoreline [*Falqués and Calvete*, 2005] (Figure 2). The constants d and B are chosen by prescribing the shoreline slope, β_s, and the water depth, D_1, at a certain offshore distance, x_1,

$$\frac{2}{3}Bd^{-1/3} = \beta_s , \quad B\left((x_1+d)^{2/3} - d^{2/3}\right) = D_1 . \tag{13}$$

For the perturbed bathymetry, we use an exponential-type shape function that tends to zero at the position of the depth of closure, $x = x_c$,

$$f(x) = \frac{e^{-x/b} - e^{-x_c/b}}{1 - e^{-x_c/b}} . \tag{14}$$

The b parameter is the e-folding length of the exponential decay. However, if b is comparable or larger than x_c, $f(x)$ decays in a linear way (approximately) between 0 and x_c. The default values used for this bathymetry are $\beta_s = 0.03$, $x_1 = x_c = 700$ m, and $D_1 = D_c = 10$ m. In addition to the shoreline slope, β_s, the mean shoreface slope β will be used. We define it as the averaged slope from shore to the wave base, i.e., the location where $D = \lambda_0/2$, and it depends both on the bathymetry and the waves. Notice that in case of planar profile, $\beta = \beta_s$. Figure 2 shows the default Dean-type profile with the two slopes used in this study.

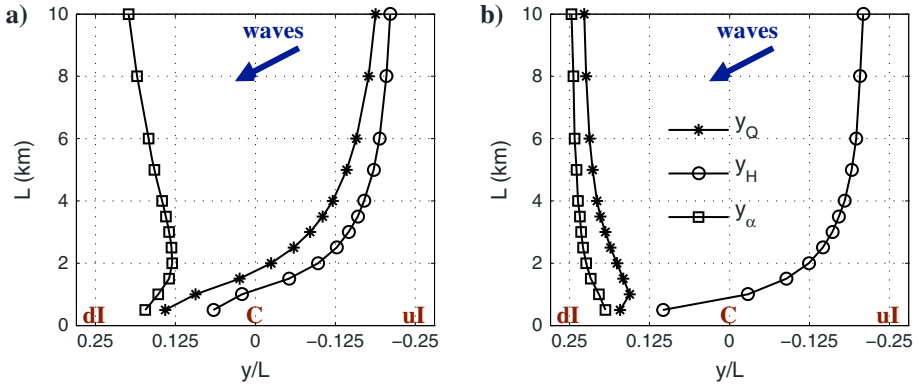

Figure 4. Alongshore location of the maximum of Q (y_Q), of H_b (y_H), and of α_b (y_α) as a function of the wavelength, L for (a) unstable conditions, $\theta_0 = 60°$ and (b) stable conditions, $\theta_0 = 30°$. The y axis increases to the left following the coordinate system of the model, $y/L = 0$ corresponds to the sand wave crest, and the region between dI and uI of Figure 1 is plotted. The model setup and parameter values are those of section 3 (Table 2).

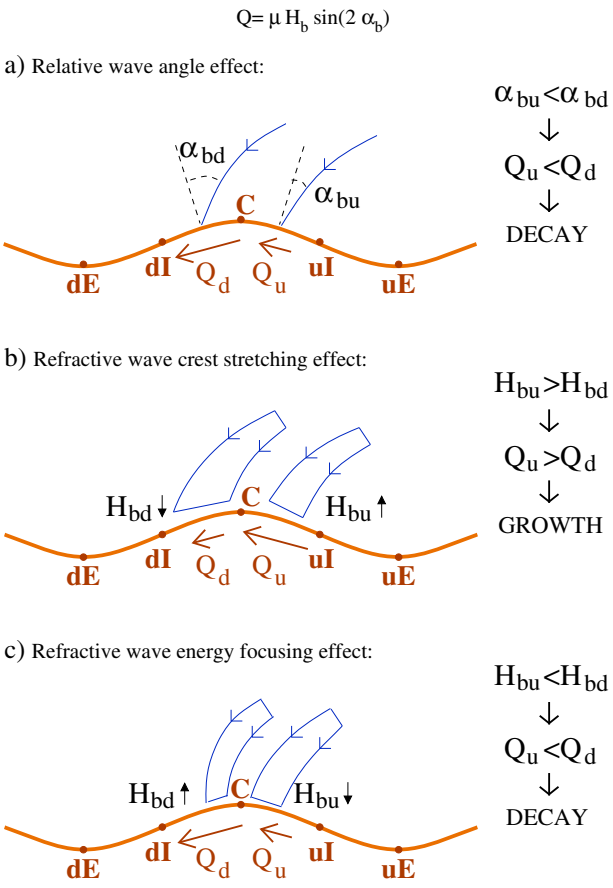

Figure 5. Sketch of the three processes governing the mechanism for wavelength selection of self-organized shoreline sand waves. The sinusoidal sand wave and the notation of Figure 1 is used (hence, u means updrift and d means downdrift).

3. Why a Wavelength Selection?

The existence of a wavelength selection for modeled self-organized shoreline sand waves of small amplitude can be illustrated with an instability curve (growth rate, σ_r, as a function of wavelength, L), like the one shown in Figure 3. It can be seen that there is a lower limit in the wavelengths (minimum or cutoff wavelength, $L = L_c$), below which sand waves decay. For $L > L_c$ sand waves grow, and they reach a maximum growth rate for $L = L_M$. For $L > L_M$ the growth rate decreases and σ_r tends asymptotically to 0 for $L \to \infty$. In the example shown in Figure 3, $L_c = 1.8$ km and $L_M = 2.5$ km. In this section we try to understand the physical mechanisms leading to this behavior. For the model simulations of this section, the Dean-type profile defined in section 2.3.2 has been used with a bathymetric perturbation given by $b = 500$ m and $x_c = 700$ m ($D_c = 10$ m). The offshore wave conditions are $H_0 = 1$ m, $\theta_0 = 60°$ and $T = 6$ s at a water depth of 10 m (Table 2).

3.1. Growth Rates for Long Sand Waves

In the limit of very long sand waves, the alongshore distance over which the orientation of the bathymetric contours changes significantly tends to be much larger than the characteristic distance over which onshore wave transformation takes place. In this situation, the bathymetric contours can be assumed rectilinear and parallel, and the simplified analysis of *Ashton et al.* [2001] is valid. In such an approach, the equation governing small-amplitude sand waves is a diffusion equation whose diffusivity is negative in the unstable case [*Murray and Ashton*, 2003; *Falqués*, 2003; *Ashton and Murray*, 2006a]. Therefore, for long sand waves the sand wave growth rate should follow a diffusive scaling and tend to zero as L^{-2}. Figure 3 shows that this is indeed the case in the present analysis, since the growth rate computed with the model (solid line) collapses to the L^{-2} fit (dashed line) for large wavelengths. In contrast, Figure 3 also shows that for intermediate to short sand waves there is a dramatic difference: for the diffusion equation [*Murray and Ashton*, 2003; *Falqués*, 2003] the growth rates increase without bound for $L \to 0$, while in the present analysis they reach a maximum ($L = L_M$) and then decrease to negative values for $L < L_c$. The next two sections are devoted to understanding this difference.

3.2. Growth Rates for Short to Intermediate Sand Waves

3.2.1. Alongshore Gradients in *Q*

To get insight into the existence of both L_c and L_M we first analyze the gradients in Q caused by a small-amplitude sinusoidal sand wave with wavelength L superimposed on an otherwise rectilinear coastline (see a sketch in Figure 1). The crest of the sand wave is located at point C ($y = 0$), the updrift and downdrift embayments are at uE ($y = -L/2$) and dE ($y = L/2$), respectively, and the corresponding updrift and downdrift inflection points are at uI ($y = -L/4$) and dI ($y = L/4$). Both the perturbation in the shoreline orientation and the perturbation in the wavefield induced by the perturbed bathymetry creates alongshore gradients in the sediment transport rate Q. Since the sand wave amplitude is small, the alongshore distribution of Q consists of an average plus a small sinusoidal perturbation of the same wavelength, L.

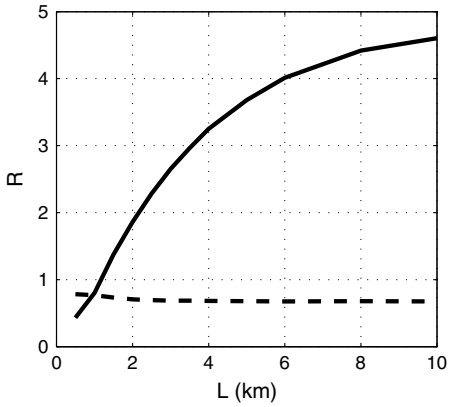

Figure 6. Relative importance of the gradients of H_b and the gradients of α_b on the gradients of Q, as a function of the wavelength, L. The ratio $R = D_H \Delta H_b / D_\alpha \Delta \alpha_b$ is plotted, where D_H and D_α are the coefficients in equation (15), and ΔH_b and $\Delta \alpha_b$ are the maximum alongshore variations of H_b and α_b, respectively. Both the case of unstable ($\theta_0 = 60°$, solid line) and stable ($\theta_0 = 30°$, dashed line) conditions are represented. A small sand wave of amplitude $A = 33$ m has been assumed. The model setup and parameter values are those of section 3 (Table 2).

If a maximum in Q is located at ul (and the minimum at dl), the minimum (negative value) in $\partial Q/\partial y$ is at C, whereas maxima in $\partial Q/\partial y$ occur at uE and dE. According to the sediment conservation equation (1), this leads to maximum accretion at C and maximum erosion at uE and dE, so that the sand wave will grow without translating. If a maximum in Q occurs between ul and C (situation represented in Figure 1), the minimum in $\partial Q/\partial y$ shifts downdrift, in between C and dl, so that the sand wave will grow and translate downdrift. Thus, the position of the maximum in Q with respect to uE, ul, C, dl, and dE determines the growth/decay and translation of the sand wave. Applications of this simple analysis can be found in *Falqués and Calvete* [2005], *List and Ashton* [2007], and *van den Berg et al.* [2012].

The position of the maximum in Q, y_Q, as a function of L is shown in Figure 4a for unstable conditions. For very small L, the maximum is located downdrift of the crest so that the sand wave decays and migrates downdrift. As L increases, y_Q moves updrift and for $L = 1.75$ km it shifts updrift of the crest. This means that the sand wave will grow, consistent with Figure 3. For larger L, y_Q moves further updrift at a decreasing rate and, for $L \geq 10$ km, it seems to stay somewhat downdrift of the updrift inflection point (ul), $y_Q \simeq -0.19L$.

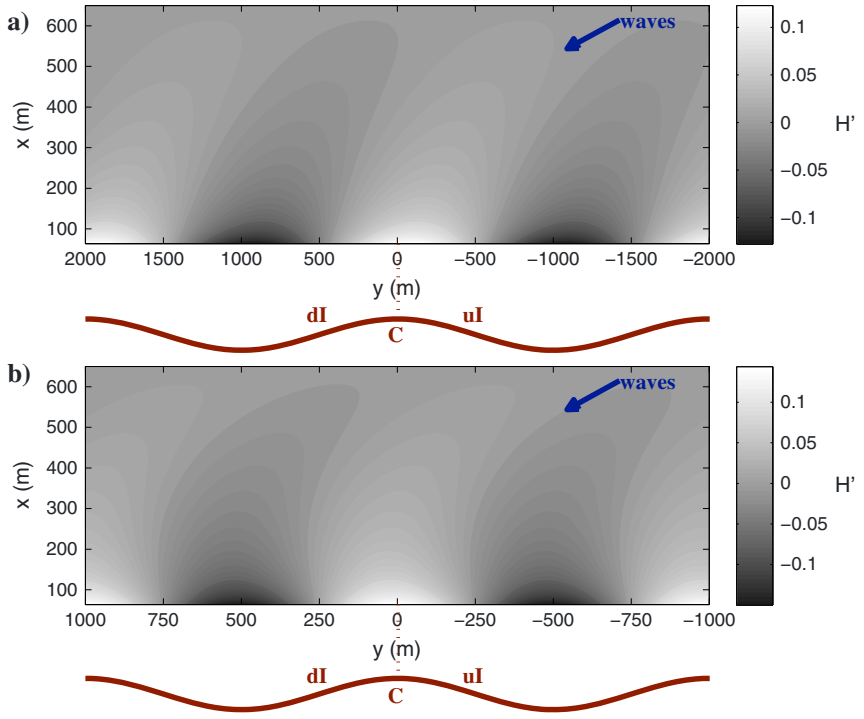

Figure 7. Perturbations in the wave height for very oblique wave incidence, $H'(x, y)$, from deep water up to breaking, for (a) $L = 2$ km (unstable wavelength), and for (b) $L = 1$ km (stable wavelength). The minimum value of the x axis ($x = 64$ m) corresponds to the mean breaking line. The sand wave shape is indicated by a brown line (crest at $y = 0$). A small sand wave of amplitude $A = 33$ m has been assumed. The model setup and parameter values are those of section 3 (Table 2).

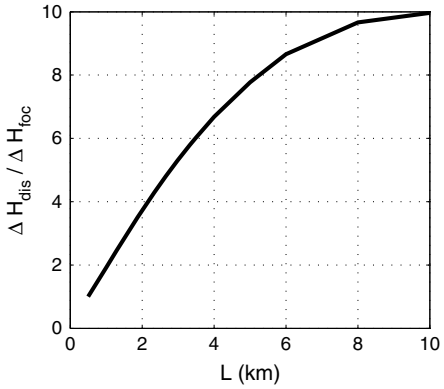

Figure 8. Relative influence of wave energy dispersion versus wave energy focusing, measured by the ratio $\Delta H_{dis}/\Delta H_{foc}$, as a function of wavelength, L. A small sand wave of amplitude $A = 33$ m has been assumed. The model setup and parameter values are those of section 3 (Table 2).

Let us now look to the physical processes behind the behavior of y_Q. According to equation (2), Q is proportional to $H_b^{5/2}$ and $\sin(2\alpha_b)$. Thus, y_Q is related to the position of the maxima in H_b ($y = y_H$) and α_b ($y = y_\alpha$) within $-L/2 \leq y \leq L/2$, which are also plotted as a function of L in Figure 4 (left). As can be seen, the maximum in Q is always located between these maxima, $y_H < y_Q < y_\alpha$. Since $\alpha_b = \theta_b - \phi$ and θ_b is relatively small, y_α is always located near the position of the minimum in ϕ, which is exactly at the inflection point dI ($y = 0.25L$). Thus y_α remains somewhat updrift of dI with small changes that depend on θ_b. Figure 5a shows a sketch that illustrates this process. In contrast, the position of the maximum in H_b moves updrift from $y_H = 0.07L$ for $L = 0.5$ km to $y_H = -0.21L$ for $L = 10$ km. This means that for very short sand waves the maximum in wave height is located slightly downdrift of the crest, while for long sand waves it is located near the uI inflection point.

The location y_Q reacts to the locations y_α and y_H depending on L (Figure 4a). For small wavelengths ($L = 0.5$ km) y_Q is closer to y_α than to y_H. In contrast, for increasing L, y_Q follows the updrift shift of y_H and moves closer to y_H. In other words, for small L the maximum in Q is controlled by the maximum in α, whereas for large L it is controlled by the maximum in H. This behavior can be understood by computing the relative importance of the alongshore variations in H_b and α_b. According to equation (2) small perturbations H_b' and α_b' will cause a small perturbation in Q of the form

$$Q' = \mu H_b^{5/2}\left(\frac{5}{2}\frac{(\sin 2\alpha_b)}{H_b}H_b' + 2\ (\cos 2\alpha_b)\alpha_b'\right) = D_H H_b' + D_\alpha \alpha_b' . \quad (15)$$

where D_H and D_α are the corresponding terms in the middle of the equation. Then, the relative importance of the variations in H_b and α_b can be estimated with the ratio $R = D_H\Delta H_b/D_\alpha\Delta\alpha_b$, where ΔH_b and $\Delta\alpha_b$ are the maximum alongshore variations of H_b and α_b, respectively. Despite equation (15) is valid in the limit of sand waves of infinitesimal amplitude, in order to estimate the quantities ΔH_b and $\Delta\alpha_b$ we have computed the wave propagation (H' and α') over the undulating bathymetry linked to a shoreline sand wave with a wavelength L and a finite cross-shore amplitude A. To make this compatible with the theoretically infinitesimal amplitude, the value chosen for A is small ($A = 33$ m) so that it verifies $A << L$. The ratio R is represented as a function of L in Figure 6. For small L, both terms are comparable (i.e., gradients in H_b and α_b play a similar role), whereas for moderate to large L, $D_H\Delta H_b \gg D_\alpha\Delta\alpha_b$ (i.e., the gradients in Q are controlled by the gradients in H_b).

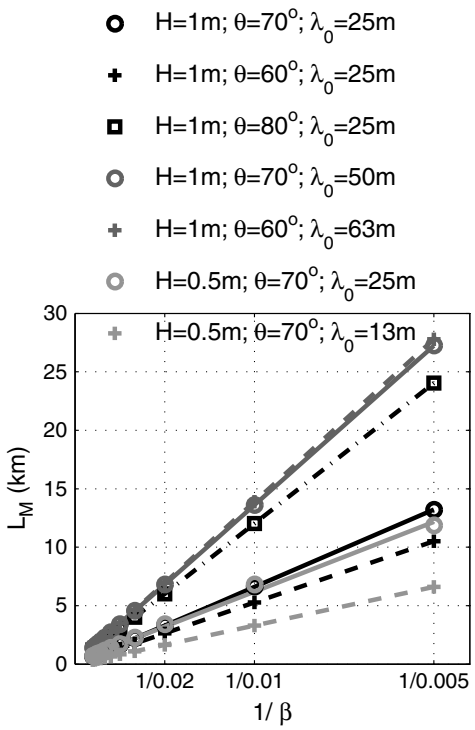

Figure 9. Sand wave dominant wavelength, L_M, as a function of the inverse of the shoreface slope, β^{-1}, for the idealized planar bathymetry, several values of the offshore wave conditions and the default values of section 4.1 for the other parameters (Table 2). The symbols correspond to model runs and the solid lines are linear fits.

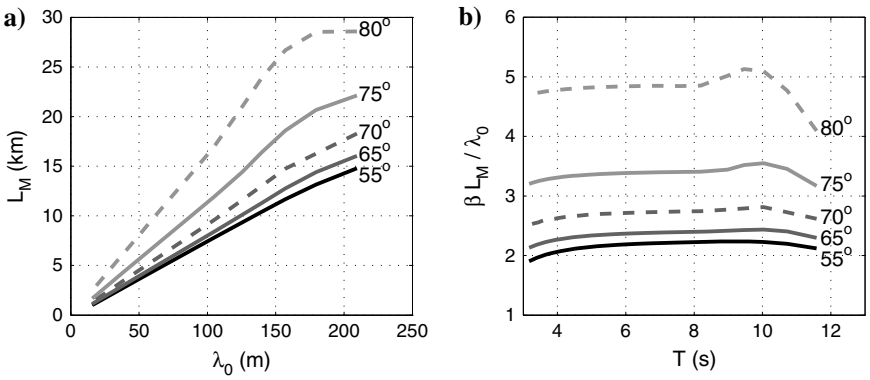

Figure 10. (a) Sand wave dominant wavelength, L_M, as a function of the wavelength of the offshore water waves, λ_0. (b) Ratio $\beta L_M/\lambda_0$ as a function of the wave period, T. The idealized planar bathymetry, several values of the wave angle, θ_0, and the default values of section 4.1 for the other parameters (Table 2) have been used for both plots.

It is interesting to compare the positions of the maxima y_H and y_α under very oblique wave incidence (i.e., the results for unstable conditions discussed above) with the positions for low-wave incidence angle (e.g., $\theta_0 = 30°$) where sand waves do not grow for any L (stable conditions). As can be seen in Figure 4b, for low-wave incidence angle, even though y_H has a similar behavior when L increases (shifting from downdrift of C to almost ul), y_Q always remains downdrift of C, following y_α, which causes decay of the sand waves. Thus, in contrast with the high incidence angle case, the maximum in Q is now dominated by the maximum in α_b for any L. Accordingly, for low-wave incidence angle the gradients in H_b and α_b play a similar role ($R \simeq 1$) for all the values of L, as shown in Figure 6. This confirms the physics of the instability mechanism that was suggested in previous studies [e.g., *Ashton and Murray*, 2006a; *Falqués et al.*, 2011; *van den Berg et al.*, 2012]: for low-wave incidence angles the gradients in Q are dominated by the gradients in α_b, leading to stability for any L (as sketched in Figure 5a), while for high angles they are dominated by the gradients in H_b, leading to instability for a certain range of L.

It should be remarked that the present discussion excludes the case of normal or nearly normal wave incidence and a very steep nearshore slope. Under these latter conditions, *Idier et al.* [2011] showed that the maximum in relative wave angle y_α can be updrift of the crest due to a very strong refraction process, and this creates convergence of sediment flux at the crest. This mechanism can lead to a different shoreline instability with a smaller length scale (O (0.1–1 km)) that could explain the formation of megacusps.

3.2.2. Alongshore Gradients in Wave Height

It is now clear that the existence of both L_c and L_M rely on how the gradients in Q depend on L and that for unstable conditions they are dominated by the alongshore gradients in $H_b(y)$. To close our investigation let us finally look into the physical reasons for the differences in the gradients in $H_b(y)$ for stable and unstable wavelengths. Figure 7 shows the perturbations in the wave height $H'(x, y)$ for the cases $L = 2$ km (unstable) and $L = 1$ km (stable). The small sand wave of amplitude $A = 33$ m has been again assumed. For very short sand waves the maximum in H_b' is located slightly downdrift of C. In contrast, for larger wavelengths the maximum in H_b' shifts updrift of the crest, between ul and C. The position of the maximum in wave energy is governed by the competition between two opposite effects. On the one hand, the refractive wave crest stretching causes an energy dispersion that is more intense when the wave ray bending is stronger (i.e., this effect is maximum at dl and minimum at ul, as sketched in Figure 5b). This process explains why the maximum in H_b' is shifted toward ul for

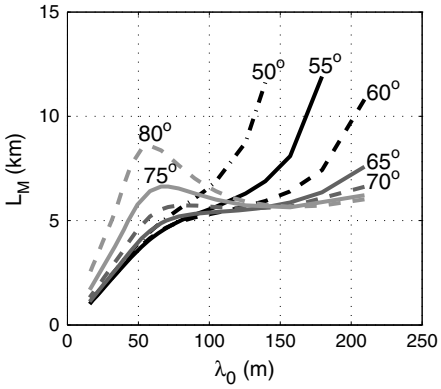

Figure 11. Sand wave dominant wavelength, L_M, as a function of the offshore water wave wavelength, λ_0, for $D_c = 30$ m. The idealized planar bathymetry, several values of the wave angle, θ_0, and the default values of section 4.1 for the other parameters (Table 2) have been used.

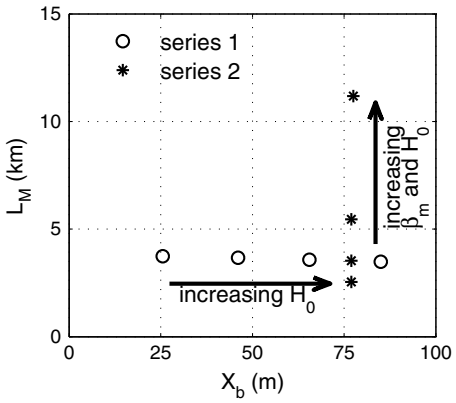

Figure 12. Influence of the surf zone width, X_b, on the sand wave wavelength, L_M. All the computations are for $\lambda_0 = 50$ m. Series 1 (circles): changing X_b with constant $\beta = 0.03$ and variable $H_0 = 0.5, 1, 1.5, 2$ m. Series 2 (asterisks): changing $\beta = 0.01, 0.02, 0.03, 0.04$ and $H_0 = 0.5, 1.13, 1.79, 2.47$ m, so that each pair of β and H_0 gives a constant $X_b = 77$ m. The idealized planar bathymetry and the default values of section 4.1 for the other parameters (Table 2) have been used.

unstable conditions, and thereby it is the main cause for the occurrence of HAWI [*Ashton and Murray*, 2006a; *Falqués et al.*, 2011; *van den Berg et al.*, 2012]. On the other hand, wave refraction also focuses wave energy near the crests, bringing the maximum in H_b' near C (exactly at C for normal wave incidence and somewhat downdrift for oblique wave incidence, as sketched in Figure 5c).

The obtained behavior of the alongshore maximum in H_b' suggests that the wave-focusing effect is dominant for very short sand waves, whereas the wave energy dispersion effect plays a stronger role for intermediate to long sand waves. In order to quantify this, we have estimated the relative importance of both effects as a function of L (Figure 8). For oblique wave incidence on an undulating coastline both effects are mixed, and it is not easy to isolate them. To make this estimate, we have then considered two situations: (a) normal wave incidence on the undulating shoreline with a given L (where there is wave focusing but not the energy spreading of the oblique incidence case) and (b) rectilinear coastline with oblique wave incidence (where there is no focusing at all). To estimate the intensity of the wave-focusing effect we compute the difference between H_b at the crests and at the embayments, $\Delta H_{\text{foc}} = H_b(y = 0) - H_b(y = L/2)$ for situation a). The intensity of the wave energy dispersion effect can be estimated by comparing H_b at the updrift flank of a crest with H_b at the downdrift flank. For this, we first evaluate the average sand wave slope, between dI and C, $\bar{\phi} = 2A/(L/2) = 4A/L$ (again, a small sand wave of amplitude $A = 33$ m has been assumed). Then, the wave height at the updrift flank, H_{bu}, is computed assuming rectilinear coast (situation b)) and an offshore wave angle $\theta_0 - \bar{\phi}$. Similarly, the wave height at the downdrift flank, H_{bd}, is computed by assuming rectilinear coast and an offshore wave angle $\theta_0 + \bar{\phi}$. Finally, the difference in wave height between the updrift and the downdrift flanks, $\Delta H_{\text{dis}} = H_{bu} - H_{bd}$, gives a measure of the intensity of the energy dispersion effect. As shown in Figure 8, the ratio $\Delta H_{\text{dis}}/\Delta H_{\text{foc}}$ is nearly 1 for small L and increases up to about 10 for $L = 10$ km. Thus, both effects are comparable for small L (~ 0.5 km), but the wave energy dispersion effect becomes dominant as L increases. The reason is that both ΔH_{dis} and ΔH_{foc} decrease for increasing L but ΔH_{foc} decreases much faster. Notice that the wave energy focusing is totally neglected in the simple approach of *Ashton et al.* [2001], where the curvature of the coastline was ignored, and this is the reason that there was not a wavelength selection in that model.

4. Basic Parametric Trends of the Dominant Wavelength

4.1. Idealized Shoreface Bathymetry: Planar Profile

After revealing the physical reasons for the existence of a dominant wavelength in model-predicted self-organized sand waves, the following step is to find out the basic length scale that controls the value of such wavelength. In order to do so, we investigate the essential parametric trends of the dominant wavelength and, as a first step, we avoid introducing length scales that are not essential to HAWI development and that could mask the fundamental dependences. Therefore, we consider the idealized planar bathymetry defined in section 2.3.1. An important parameter is the depth of closure, D_c, whose order of magnitude in nature is O (10m). However, we have found that using values in the realistic range introduces a length scale that interferes with other important length scales of the problem. In order to avoid this effect an unrealistically large depth of closure, $D_c = 100$ m, is used as default value in the present section, and the effect of using smaller values is investigated later on.

The sensitivity analysis is done in terms of the shoreface slope, β, and the offshore wave height, angle, and period (H_0, θ_0, and T), and the influence of the breaking index (γ_b) is also investigated. The default values of the water wave parameters are the same as in section 3 (Table 2). Consistently with *Falqués and Calvete*

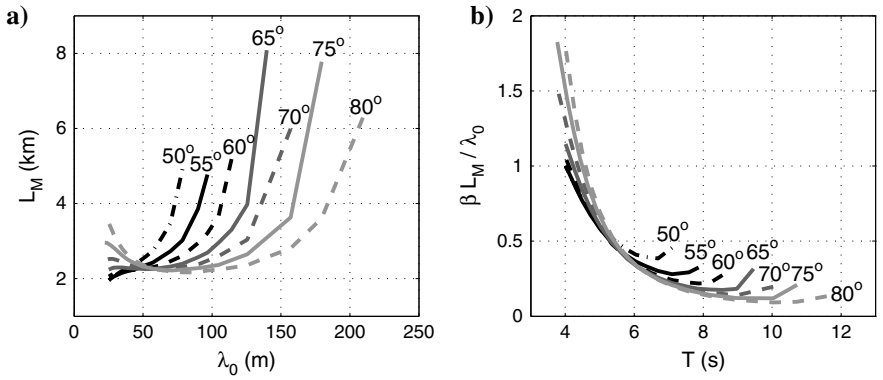

Figure 13. (a) Sand wave dominant wavelength, L_M, as a function of the wavelength of the offshore water waves, λ_0. (b) Ratio $\beta L_M/\lambda_0$ as a function of the wave period, T. The Dean-type bathymetry, several values of the wave angle, θ_0, and the default values of section 4.2 for the other parameters (Table 2) have been used for both plots.

[2005], it is found that if θ_0 is large enough and T is small enough, the growth rates are positive for a certain range of sand wave wavelengths, L (an example can be seen in Figure 3).

The sand wave dominant wavelength (L_M), is inversely proportional to the slope (β), as shown in Figure 9 for different offshore wave conditions. The corresponding linear fits show high correlation coefficients, $R^2 > 0.999$. Given a value of β, θ_0, and H_0, L_M is roughly proportional to the water wavelength, λ_0 (Figure 10a). The relationship is linear for moderate angles ($50° < \theta_0 \leq 70°$) and deviates from linearity for large λ_0 in case of very large angles ($\theta_0 > 70°$). Thus, taking also into account the proportionality between L_M and β, the ratio $\beta L_M/\lambda_0$ remains relatively constant for each wave angle. This quantity is in the range 2–2.5 for moderate angles and rises up to about 5 for very large angles, as shown in Figure 10b.

The relationship between L_M and λ_0 also depends on D_c. If smaller values are considered for the latter, the former relationship deviates gradually from linearity when T increases and this is more pronounced for large θ_0. Figure 11 shows that relationship for $D_c = 30$ m, and it can be seen that linearity only holds up to $\lambda_0 \simeq 60$ m, i.e., up to $\lambda_0/2 \simeq D_c$. The reason could be that short water waves ($\lambda_0/2 < D_c$) only feel the perturbed depth contours, whereas long water waves ($\lambda_0/2 > D_c$) waves feel both the perturbed and the unperturbed bathymetry.

An interesting issue is the dependence of L_M on the width of the surf zone (X_b) since previous studies had suggested that L_M is roughly proportional to X_b [*Falqués and Calvete*, 2005; *Uguccioni et al.*, 2006]. Two series of experiments are carried out. In the first one, we change the wave height, H_0 (=0.5, 1, 1.5, and 2 m), and we keep λ_0 and β constant at 50 m and 0.03, respectively. In this way, X_b varies from 25.5 to 85 m but L_M hardly changes (Figure 12). In the second series, we change both H_0 (=0.5, 1.13, 1.79, and 2.47 m) and β (= 0.01, 0.02, 0.03, and 0.04) in order to keep X_b fixed at 77 m. The water wavelength is again $\lambda_0 = 50$ m. In this situation, L_M changes from 2.55 km to 11.18 km. This demonstrates that, in contrast with the earlier suggestions, L_M does not depend on X_b. Those earlier assumptions were likely based on the fact that for a constant H_0, an increase in X_b can be obtained by a decrease in β, which does cause an increase in L_M.

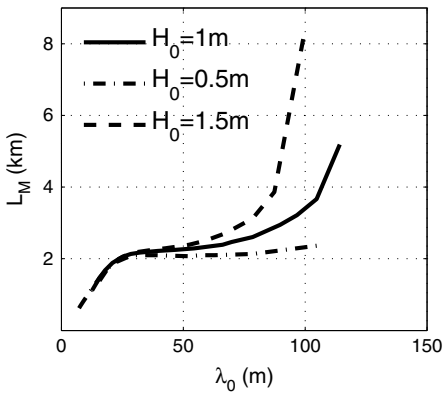

Figure 14. Relationship between L_M and λ_0 for the Dean-type bathymetry, several values of the wave height, H_0, and the default values of section 4.2 for the other parameters (Table 2).

Finally, there is little influence of the breaking index, γ_b, on the sand wave wavelength. This is found by comparing the results for $\gamma_b = 0.4, 0.6$ and 0.8. Similarly, wave height has no influence on L_M for this idealized planar bathymetry.

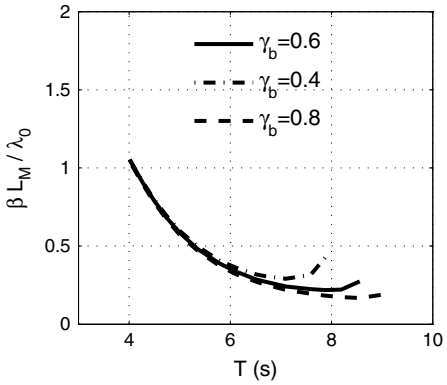

Figure 15. Relationship between the ratio $\beta L_M/\lambda_0$ and the wave period T for the Dean-type bathymetry, several values of the wave breaking index, γ_b, and the default values of section 4.2 for the other parameters (Table 2).

4.2. Realistic Shoreface Bathymetry: Dean-Type Profile

In order to investigate to what extent the behavior of real shoreface bathymetries deviates from the basic trends found in section 4.1, we now consider the more realistic Dean-type bathymetry defined in section 2.3.2, with $b = 15$ km and $x_c = 700$ m ($D_c = 10$ m). A large value of b has been chosen so that the bathymetric perturbation decays in a linear way from shore to the depth of closure. The dependence of L_M on the slope is explored by keeping the shape of the profile fixed. Thus, when the shoreline slope, β_s, is increased or decreased, D_1 is varied in the same proportion. If L_M is then plotted against the mean shoreface slope β (averaged from shore to the wave base), for the same wave conditions used in Figure 9, all the lines are also approximately straight (not shown). Again, the two quantities show a clear linear correlation, with $R^2 > 0.99$.

Figure 13a shows that the relationship between L_M and λ_0 is more complex than in the previous section. This is probably due to the fact that for $D_c = 10$ m the waves feel both the perturbed and the unperturbed bathymetric contours (see section 4.1) for all the investigated wavelengths, $\lambda_0 \geq 20$ m, and the proportion of each type of bathymetry they feel depends on their wavelength. For moderate angles, $\theta_0 \simeq 50 - 65°$, L_M increases with λ_0, although not linearly. By increasing θ_0 the lines $L_M - \lambda_0$ show a more complex behavior. In spite of this complexity, the $\beta L_M/\lambda_0$ ratio as a function of the wave period, T, has a quite regular behavior as shown in Figure 13b, where all the lines corresponding to different angles almost collapse in a single one. This average line decreases with increasing wave period, but for typical wave periods in the range 6–12 s, $\beta L_M/\lambda_0$ is quite constant, in the range 0.1–0.4. For very short periods $T = 4$–5 s it increases and reaches up to 1.8.

The relationship between L_M and the width of the surf zone, X_b, is examined by repeating the same two series of experiments as in section 4.1 (not shown). Again, when X_b varies keeping β and λ_0 constant, L_M hardly changes. And when X_b is kept constant (and also λ_0) but β varies, L_M changes significantly. The influence of the wave height is negligible for λ_0 up to 30 m. However, in contrast with the planar bathymetry, H_0 has now some influence on L_M for larger λ_0 (Figure 14). Again, this can be probably explained by the ratio between D_c and the depth at the wave base, $\lambda_0/2$, controlling how much of the perturbed bathymetry is felt by the waves before breaking (for the planar bathymetry, $D_c = 100$ m). Similarly, there is almost no influence of γ_b on L_M for relatively short water waves but for wave periods above $T \simeq 6$ s, L_M tends to decrease for increasing γ_b (Figure 15).

5. Discussion

5.1. Scaling Law for the Dominant Wavelength

The main conclusion from the numerical experiments of section 4 is that the HAWI dominant wavelength, L_M, scales with the water wavelength, λ_0, and is inversely proportional to the mean shoreface slope, β, according to

$$L_M = c(\theta_0, \lambda_0, H_0)\frac{\lambda_0}{\beta} \tag{16}$$

where the factor c is typically in the range 0.1–0.4 and up to 1.8 for very short periods (using the more realistic Dean-type bathymetry).

In order to interpret this scaling law of the dominant wavelength, we have performed a scaling of the model equations. We know that the existence of a dominant wavelength of the sand waves is related with the gradients of the wave energy along the undulating shoreline (section 3). In other words, the wavelength selection is controlled by some properties of wave refraction and shoaling over sinusoidal depth contours. Thus, to get insight into the origin of such alongshore length scale it is convenient to scale the wave transformation equations (4)–(6), disregarding the morphodynamic equations (1) and (2).

Given the undisturbed bathymetric profile, $D_0(x)$, we define the horizontal cross-shore length scale, L_x, and the mean shoreface slope, β, averaged from shore to the wave base (Figure 2), by

$$D_0(L_x) = \lambda_0\,, \quad \beta = \frac{\lambda_0}{L_x}\,. \tag{17}$$

It is assumed that seaward of the surf zone $D_0(x)$ is a monotonically increasing function. Since the wave base is typically defined by $D_0 \simeq \lambda_0/2$, L_x gives roughly an indication of the order of magnitude of the distance that the waves need to travel in order to undergo appreciable transformation. We also introduce a horizontal alongshore length scale, L_y, which will be specified later. The scaling is then defined by

$$x = L_x\hat{x}\,, \quad y = L_y\hat{y}\,, \quad D = \lambda_0\hat{D}\,, \quad k = \lambda_0^{-1}\hat{k}\,, \quad H = \lambda_0\hat{H}\,, \tag{18}$$

where the hat indicates nondimensional quantities. Notice that according to equations (17) and (18), $\hat{D}_0(1) = 1$, no matter the values of λ_0 and β. Applying the scaling to the water wave equations (4)–(6) gives

$$2\pi = \hat{k}\,\tanh(\hat{k}\hat{D})\,, \tag{19}$$

$$\frac{L_y}{L_x}\frac{\partial}{\partial\hat{x}}(\hat{k}\sin\theta) = \frac{\partial}{\partial\hat{y}}(-\hat{k}\cos\theta)\,, \tag{20}$$

$$\frac{L_y}{L_x}\frac{\partial}{\partial\hat{x}}(-\hat{c}_g\hat{H}^2\cos\theta) + \frac{\partial}{\partial\hat{y}}(\hat{c}_g\hat{H}^2\sin\theta) = 0\,. \tag{21}$$

The integration domain becomes $\hat{x} \geq \hat{x}_b(\hat{y}, t)$ such that $\hat{H}(\hat{x}_b, \hat{y}, t) = \gamma_b\hat{D}(\hat{x}_b, \hat{y}, t)$, and the boundary conditions are

$$\hat{k}(\infty, \hat{y}, t) = 2\pi\,, \quad \theta(\infty, \hat{y}, t) = \theta_0\,, \quad \hat{H}(\infty, \hat{y}, t) = \frac{H_0}{\lambda_0}\,. \tag{22}$$

The original form of the water wave equations (4)–(6) and the boundary conditions (equation (7)) is met if one chooses $L_y = L_x$. This means that any combination of the parameters that keep θ_0, H_0/λ_0, and γ_b invariant will give the same nondimensional solution provided that $L_y = L_x$. Therefore, according to equation (17), the natural alongshore length scale is

$$L_y = \frac{\lambda_0}{\beta}\,, \tag{23}$$

which is consistent with the scaling law for the dominant wavelength L_M that we have found with the model (equation (16)). It is important to note that multiplying the depth profile $D_0(x)$ by a constant changes β, and hence L_x and L_y, but it does not change the form of the solution for the wave field.

This scaling explains why for open ocean beaches L_M is so large (Table 1). For $\lambda_0 \sim 100$ m and $\beta \sim 0.002$, the scale L_y is 50 km, while for $\lambda_0 \sim 20$ m and $\beta \sim 0.01$ it is 2 km, i.e., much larger than the width of the surf zone. Applying equation (16) for a realistic shoreface profile with the appropriate values of c, one obtains wavelengths in the range 1–10 km.

5.2. Model Limitations

The objectives of this study were to unravel the physical reasons for the existence of a model-predicted wavelength selection and to find out the main parametric trends of the dominant wavelength. In order to get insight into the fundamental processes, we have used a simple approach: one-line shoreline modeling and geometric optics approximation for wave refraction and shoaling. An important improvement would be to study sand wave formation under a wave field including wave spreading, i.e., with a distribution of wave angles and periods. For this, a more sophisticated wave model, like a spectral model, should be used. The limitations of the one-line modeling approach do not seem to be essential since the present results on wavelength selection are qualitatively similar to those obtained by using a nonlinear quasi 2-D model [see *van den Berg et al.*, 2012]. Moreover, the preliminary results of *List and Ashton* [2007] suggest that computing Q with the CERC formula, as we have done, or from a fully 2-D hydrodynamically based model (Delft3D) gives qualitatively similar results.

Finally, we should mention that the present study has been based on the existence of a single maximum in the instability curve. However, for a marginal region in the parameter space, such as for very high angle (e.g., $\theta_0 \gtrsim 70°$) and for some combinations of bathymetric profile and wave period, the instability curve can show a more complex behavior, with secondary maxima for relatively short wavelengths ($L \sim 1$ km, not shown). This behavior was also found by *Uguccioni et al.* [2006], and it was interpreted as a result of wave rays crossing several bathymetric undulations and this only occurs when the wavelength of the sand waves is small, the wave obliquity is very high or the wave period is very short.

5.3. How Can Model Predictions be Tested?

The present study has been entirely set up at the modeling level to understand how the processes involved in HAWI can lead to an initially most preferred wavelength for shoreline sand waves. In order to validate the model results with experimental data two aspects of the study could be explored: (i) the scaling prediction of equation (16) and (ii) the identified essential physical processes.

It is important to realize that equation (16) only gives a basic scaling and not a precise prediction of the wavelength. This is because the model computations have been done only for two very simple bathymetric profiles, which are alongshore uniform, and for a limited range of wave conditions. Furthermore, the model is based on linear stability analysis so that it refers to the initial tendency of sand waves to grow while the wavelength of finite amplitude sand waves in the field can deviate substantially from the one given by equation (16). The best scenario for such comparison would be coasts that are at the brink of instability. For instance, larger-scale features developed under high-angle waves tend to reorientate the updrift coast to be at the threshold for instability [*Ashton et al.*, 2001] such that fluctuations in wave climate can lead to the formation of small-amplitude sand waves there. Recently, D. Idier and A. Falqués (How kilometric sandy shoreline undulations correlate with wave and morphology characteristics: Preliminary analysis on the atlantic Coast of Africa, submitted to *Advances in Geosciences*, 2013) examined the validity of the estimate given by equation (16) for the kilometer-scale shoreline sand waves along 4500 km of the west coast of Africa. They used global data of shoreline shapes to obtain the sand wave wavelengths, global bathymetries to obtain the mean shoreface slopes, and global wave climate for the water wave wavelength. Their results showed a $c = \beta L_M/\lambda_0$ ratio in the range 0.02–0.5, which is in the same order of magnitude of the values obtained with the model. As shown in Figure 13, for large wave periods (as observed on the African coast) $c \sim$ 0.1–0.4. A more precise prediction of the initial wavelength on a particular coast would require the use of the specific bathymetry and wave conditions of that site. But even in this case, the model assumes alongshore uniformity and this is hardly found in nature.

The validation of the processes behind wavelength selection could be done by measuring the distribution of wave height and relative wave angle at breaking along an undulating shoreline with similar undulating bathymetric contours. This could be done directly in the field for different wave conditions. In this way, the location of the maximum in wave angle, which should be close to the downdrift inflection point (see Figure 4), could be checked. The matter is not so easy regarding the wave height. According to the model the maximum in wave energy moves from downdrift of the crest to close to the updrift inflection point by increasing the sand wave wavelength. This cannot be checked by looking just to a particular sand wave site with a specific wavelength. However, the wavelength of real sand waves very often displays some alongshore variability, and this can be used to examine how the relative position of the maximum in wave energy depends on sand wave wavelength. Moreover, according to equation (16), the effect of increasing sand wave wavelength should be equivalent to reducing water wave wavelength, which is achieved by the natural variability in wave conditions. In other words, on a sand wave train with $L = 2$ km switching from waves with $\lambda_0 = 100$ m to waves with $\lambda_0 = 50$ m would correspond, regarding the relative position of the maximum in wave height, to looking to $L = 4$ km for $\lambda_0 = 100$m. Notice however that the effective setup of the experiments would not be straightforward at all since wave height and direction can vary locally at a smaller scale than sand waves (sand bars, rip channels, etc.) and in time. So to get average patterns, several points and a long period would be needed so that a large array of instruments in different alongshore locations would be necessary. Thereby, to check the alongshore distributions of wave height and angle, the ideal experimental setup would be a 2-D wave tank with nonerodible undulating bottoms with a number of different wavelengths. According to the scaling given by equation (16), for waves of $T \simeq 1$ s on a sloping shoreface with $\beta = 0.1$, this is feasible because the relevant wavelengths for the tests would be roughly in the range 5–30 m.

6. Conclusions

Several model studies show that self-organized shoreline sand waves triggered by very oblique wave incidence initially develop with a preferred wavelength in the range 1–10 km, which is quite common for observed sand waves in many coasts. The physical mechanisms that explain this wavelength selection have been quantified. In agreement with previous studies, the onset of the instability is governed by an interplay of two physical effects: (a) largest relative (to the local shoreline) wave angle at the downdrift flank of the sand wave and (b) wave energy concentration at the updrift flank due to less refractive energy dispersion. Effect (a) brings the maximum sediment transport rate Q downdrift of the crest thereby causing divergence of flux at the crest and decay of the sand wave. In contrast, effect (b) brings the maximum in Q at the updrift flank causing convergence of flux at the crest and growth of the sand wave. These processes can be slightly modified by the curvature of the bathymetric contours, but they do not depend essentially on it. They both are described by the diffusion equation of *Ashton and Murray* [2006a] where the curvature is ignored. For high-angle waves (b) is dominant thereby the shoreline is unstable and the diffusivity is negative. The growth rate is proportional to L^{-2}, tending to 0 for large wavelengths and increasing without bound for short wavelengths. The new important aspect analyzed here is a third physical effect, (c) wave energy concentration slightly downdrift of the crest due to refractive focusing. It essentially depends on the curvature of the shoreline and is crucial for wavelength selection. Indeed, for large wavelengths (b) is dominant while for short sand waves (c) takes over, brings the maximum in Q at the downdrift flank and the sand wave decays. Since for long sand waves the growth rates decrease to 0, there exists a maximum growth rate for some intermediate L_M. Our model investigation show that for large L the curvature becomes negligible and the growth rate approximately follows the diffusive scaling, i.e., is roughly proportional to L^{-2}.

A simple scaling of the equations governing the refraction and shoaling of waves shows that the basic alongshore length scale of shoreline sand waves equals λ_0/β, where λ_0 is the wavelength of the offshore water waves and β is the mean shoreface slope (from shore to the wave base). This scale λ_0/β is twice the distance from the wave base to the shore, and it gives an estimate of the order of magnitude of the distance that the waves need to travel in order to undergo significant refraction and shoaling. Consistently, numerical experiments confirm that the dominant wavelength, L_M, is roughly proportional to λ_0/β. In general, this proportionality holds approximately except if the wave base is deeper than the depth of closure ($\lambda_0/2 > D_c$). In the latter case the behavior of L_M with λ_0 is more complex probably because the waves feel both the unperturbed and the perturbed bathymetries in a different proportion depending on λ_0. The modeled proportionality factor for the Dean-type bathymetry typically ranges on open ocean beaches from 0.1 to 0.4 (for very low wave periods it increases and can reach, e.g., 1.8 for $T = 4$ s), and it mainly depends on the offshore angle of incident waves. The wave height only has an effect on L_M in case of a nonplanar shoreface and large wave periods. The width of the surf zone and the breaking index do not affect L_M significantly.

The scaling law for L_M obtained in this study explains why L_M is so large for open ocean beaches, in comparison with the surf zone width or the wavelength of the waves. According to this scaling law, realistic shoreface profiles with typical incoming ocean waves give wavelengths in the range 1–10 km.

Acknowledgments
This research has been funded by the Spanish government through the research projects CTM2009-11892 and CTM2012-35398 and through a FPI scholarship for the first author.

References

Alves, A. R. (2009), Long-term erosional hot spots in the southern Brazilian coast, *J. Geophys. Res.*, *114*, C02020, doi:10.1029/2008JC004933.

Ashton, A. D., and A. B. Murray (2006a), High-angle wave instability and emergent shoreline shapes: 1. Modeling of sand waves, flying spits, and capes, *J. Geophys. Res.*, *111*, F04011, doi:10.1029/2005JF000422.

Ashton, A. D., and A. B. Murray (2006b), High-angle wave instability and emergent shoreline shapes: 2. Wave climate analysis and comparisons to nature, *J. Geophys. Res.*, *111*, F04012, doi:10.1029/2005JF000423.

Ashton, A. D., A. B. Murray, and O. Arnault (2001), Formation of coastline features by large-scale instabilities induced by high-angle waves, *Nature*, *414*, 296–300.

Ashton, A. D., A. B. Murray, R. Littlewood, D. A. Lewis, and P. Hong (2009), Fetch-limited self-organization of elongate water bodies, *Geology*, *37*, 187–190.

Bruun, P. (1954), Migrating sand waves or sand humps, with special reference to investigations carried out on the Danish North Sea coast, in *Proceedings of the 5th International Conference on Coastal Engineering*, pp. 269–295, Am. Soc. of Civ. Eng., New York.

Caballeria, M., A. Falqués, and N. van den Berg (2011), Potential instabilities of Catalan coastline induced by high-angle waves, in *Proceeding of the 7th IAHR Symposium on River, Coastal and Estuarine Morphodynamics*, pp. 2133–2143, Tsinghua Univ. Press, Beijing, China. [CD-ROM].

Davidson-Arnott, R. G. D., and A. van Heyningen (2003), Migration and sedimentology of longshore sandwaves, Long Point, Lake Erie, Canada, *Sedimentology*, *50*, 1123–1137.

Falqués, A. (2003), On the diffusivity in coastline dynamics, *Geophys. Res. Lett.*, *30*(21), 2119, doi:10.1029/2003GL017760.

Falqués, A., and D. Calvete (2005), Large-scale dynamics of sandy coastlines: Diffusivity and instability, *J. Geophys. Res.*, *110*, C03007, doi:10.1029/2004JC002587.
Falqués, A., D. Calvete, and F. Ribas (2011), Shoreline instability due to very oblique wave incidence: Some remarks on the physics, *J. Coastal Res.*, *27*(2), 291–295.
Gravens, M. B. (1999), Periodic shoreline morphology, Fire Island, New York, in *Coastal Sediments '99*, edited by N. Kraus and W. McDougal, pp. 1613–1626, World Sci.
Guillen, J., M. J. F. Stive, and M. Capobianco (1999), Shoreline evolution of the Holland coast on a decadal scale, *Earth Surf. Process. Landforms*, *24*, 517–536.
Idier, D., A. Falqués, B. G. Ruessink, and R. Garnier (2011), Shoreline instability under low-angle wave incidence, *J. Geophys. Res.*, *116*, F04031, doi:10.1029/2010JF001894.
Inman, D. L., M. H. S. Elwany, A. A. Khafagy, and A. Golik (1992), Nile Delta profiles and migrating sand blankets, in *Coastal Engineering 1992*, pp. 3273–3284, Am. Soc. of Civ. Eng., Reston, Virginia, U.S.A.
Kaergaard, K., and J. Fredsoe (2013), Numerical modeling of shoreline undulations. Part 1: Constant wave climate, *Coastal Eng.*, *75*, 64–76.
Kaergaard, K., J. Fredsoe, and S. B. Knudsen (2012), Coastline undulations on the West Coast of Denmark: Offshore extent, relation to breaker bars and transported sediment volume, *Coastal Eng.*, *60*, 109–122.
Komar, P. D. (1998), *Beach Processes and Sedimentation*, 2nd ed., Prentice Hall, Englewood Cliffs, N. J.
List, J. H., and A. D. Ashton (2007), A circulation modeling approach for evaluating the conditions for shoreline instabilities, in *Coastal Sediments 2007*, pp. 327–340, Am. Soc. of Civ. Eng., Reston, Virginia, U.S.A.
Medellín, G., R. Medina, A. Falqués, and M. González (2008), Coastline sand waves on a low-energy beach at "El Puntal" spit, Spain, *Mar. Geol.*, *250*, 143–156.
Medellín, G., A. Falqués, R. Medina, and M. González (2009), Coastline sand waves on a low-energy beach at El Puntal spit, Spain: Linear stability analysis, *J. Geophys. Res.*, *114*, C03022, doi:10.1029/2007JC004426.
Murray, A. B., and A. D. Ashton (2003), Sandy-coastline evolution as an example of pattern formation involving emergent structures and interactions, in *Proceedings of the International Conference on Coastal Sediments 2003*, edited by N. J. Hackensack, World Sci., Barcelona, Spain, [CD-ROM].
Pelnard-Considère, R. (1956), Essai de theorie de l'evolution des formes de rivage en plages de sable et de galets, in *4th Journees de l'Hydraulique, Les Energies de la Mer, Paris,* vol. III(1), pp. 289–298, Société Hydrotechnique de France, Paris, Fr.
Ribas, F., A. Falqués, N. van den Berg, and M. Caballeria (2013), Modeling shoreline sand waves on the coasts of Namibia and Angola, *Int. J. Sediment Res.*, *28*(3), 338–348.
Ruessink, B. G., and M. C. J. L. Jeuken (2002), Dunefoot dynamics along the Dutch coast, *Earth Surf. Process. Landforms*, *27*, 1043–1056.
Ryabchuk, D., I. Leont'yev, A. Sergeev, E. Nesterova, L. Sukhacheva, and V. Zhamoida (2011), The morphology of sand spits and the genesis of longshore sand waves on the coast of the eastern Gulf of Finland, *Baltica*, *24*(1), 13–24.
Stive, M. J. F., S. G. J. Aarninkhof, L. Hamm, H. Hanson, M. Larson, K. M. Wijnberg, R. J. Nicholls, and M. Capobianco (2002), Variability of shore and shoreline evolution, *Coastal Eng.*, *47*, 211–235.
Thevenot, M. M., and N. C. Kraus (1995), Longshore sand waves at Southampton Beach, New York: Observation and numerical simulation of their movement, *Mar. Geol.*, *126*, 249–269.
Uguccioni, L., R. Deigaard, and J. Fredsoe (2006), Instability of a coastline with very oblique wave incidence, in *Proceedings of the 30th Coastal Engineering Conference*, pp. 3542–3553, World Sci.
van den Berg, N., A. Falqués, and F. Ribas (2011), Long-term evolution of nourished beaches under high angle wave conditions, *J. Mar. Syst.*, *88*, 102–112.
van den Berg, N., A. Falqués, and F. Ribas (2012), Modeling large scale shoreline sand waves under oblique wave incidence, *J. Geophys. Res.*, *117*, F03019, doi:10.1029/2011JF002177.
Verhagen, H. J. (1989), Sand waves along the dutch coast, *Coastal Eng.*, *13*, 129–147.